Available online at www.sciencedirect.com
ScienceDirect
Polymer 48 (2007) 530–541
polymer
www.elsevier.com/locate/polymer

Toughening mechanisms of nanoparticle-modified epoxy polymers

B.B. Johnsen [a], A.J. Kinloch [a], R.D. Mohammed [a], A.C. Taylor [a,*], S. Sprenger [b]

[a] Department of Mechanical Engineering, Imperial College London, South Kensington Campus, London SW7 2AZ, UK
[b] Nanoresins AG, Charlottenburger Strasse 9, 21502 Geesthacht, Germany

Received 11 August 2006; received in revised form 26 October 2006; accepted 16 November 2006
Available online 15 December 2006

Abstract

An epoxy resin, cured with an anhydride, has been modified by the addition of silica nanoparticles. The particles were introduced via a sol–gel technique which gave a very well-dispersed phase of nanosilica particles which were about 20 nm in diameter. Atomic force and electron microscopies showed that the nanoparticles were well-dispersed throughout the epoxy matrix. The glass transition temperature was unchanged by the addition of the nanoparticles, but both the modulus and toughness were increased. The measured modulus was compared to theoretical models, and good agreement was found. The fracture energy increased from 100 J/m^2 for the unmodified epoxy polymer to 460 J/m^2 for the epoxy polymer with 13 vol% of nanosilica. The fracture surfaces were inspected using scanning electron and atomic force microscopies, and the results were compared to various toughening mechanisms proposed in the literature. The toughening mechanisms of crack pinning, crack deflection and immobilised polymer were discounted. The microscopy showed evidence of debonding of the nanoparticles and subsequent plastic void growth. A theoretical model of plastic void growth was used to confirm that this mechanism was indeed most likely to be responsible for the increased toughness that was observed due to the presence of the nanoparticles.

Keywords: Epoxy; Nanoparticles; Fracture

1. Introduction

Epoxy polymers are widely used for the matrices of fibre-reinforced composite materials and as adhesives. When cured, epoxies are amorphous and highly-crosslinked (i.e. thermosetting) polymers. This microstructure results in many useful properties for structural engineering applications, such as a high modulus and failure strength, low creep, and good performance at elevated temperatures.

However, the structure of such thermosetting polymers also leads to a highly undesirable property in that they are relatively brittle materials, with a poor resistance to crack initiation and growth. Nevertheless, it has been well established for many years that the incorporation of a second microphase of a dispersed rubber, e.g. [1–5], or a thermoplastic polymer, e.g. [6–8], into the epoxy polymer can increase their toughness. Here the rubber or thermoplastic particles are typically about 1–5 μm in diameter with a volume fraction of about 5–20%. However, the presence of the rubbery phase typically increases the viscosity of the epoxy monomer mixture and reduces the modulus of the cured epoxy polymer.

Hence rigid, inorganic particles have also been used, as these can increase the toughness without affecting the glass transition temperature of the epoxy polymer. Here glass beads or ceramic (e.g. silica or alumina) particles with a diameter of between 4 and 100 μm are typically used, e.g. [9–14]. However, these relatively large particles also significantly increase the viscosity of the resin, reducing the ease of processing. In addition, due to the size of these particles they are unsuitable for use with infusion processes for the production of fibre composites as they are strained out by the small gaps between the fibres.

More recently, a new technology has emerged which holds promise for increasing the mechanical performance of such

* Corresponding author. Tel.: +44 20 7594 7149; fax: +44 20 7594 7017.
E-mail address: a.c.taylor@imperial.ac.uk (A.C. Taylor).

0032-3861/$ - see front matter © 2006 Elsevier Ltd. All rights reserved.
doi:10.1016/j.polymer.2006.11.038

thermosetting polymers. This is via the addition of a nanophase structure in the polymer, where the nanophase consists of small rigid particles of silica [15–18]. Such nanoparticle-modified epoxies have been shown to not only increase further the toughness of the epoxy polymer but also, due to the very small size of the silica particles, not to lead to a significant increase in the viscosity of the epoxy monomer.

The aims of the present work were to investigate the fracture toughness of epoxy polymer modified with silica nanoparticles, and to establish the structure/property relationships. The toughening mechanisms which may be operating will be reviewed, and the mechanism most likely to be responsible will be identified.

2. Experimental

2.1. Materials

The materials were based upon a one-component hot-cured epoxy formulation. The epoxy resin was a standard diglycidyl ether of bis-phenol A (DGEBA) with an epoxy equivalent weight (EEW) of 185 g/mol, 'Bakelite EPR 164' supplied by Hexion Speciality Chemicals, Duisburg, Germany. The silica (SiO_2) nanoparticles were supplied as a colloidal silica sol in the resin matrix, 'Nanopox F400', by Nanoresins, Geesthacht, Germany. The particles are synthesised from aqueous sodium silicate solution [19,20]. They then undergo a process of surface modification with organosilane and matrix exchange, to produce a masterbatch of 40 wt% (26 vol%) silica in the epoxy resin. The nanosilica particles had a mean particle size of about 20 nm, with a narrow range of particle-size distribution; laser light scattering shows that almost all particles are between 5 and 35 nm in diameter. The particle size and excellent dispersion of these silica particles remain unchanged during any further mixing and/or blending operations. Further, despite the relatively high silica content of 26 vol%, the nanofilled epoxy resin still has a comparatively low viscosity due to the agglomerate-free colloidal dispersion of the nanoparticles in the resin. The small diameter and good dispersion of the nanoparticles of silica have been previously reported and shown [15,16]. The curing agent was an accelerated methylhexahydrophthalic acid anhydride, namely 'Albidur HE 600' supplied by Nanoresins, Geesthacht, Germany.

Bulk sheets of unmodified epoxy and nanosilica-modified epoxy polymers were produced to determine the properties of the polymers. Firstly, the simple DGEBA resin was mixed together with given amounts of the nanosilica-containing epoxy resin. The value of the EEW of the blend was then measured via titration. Secondly, the stoichiometric amount of the curing agent was added to the mixture, which was poured into release-coated moulds and pre-cured for 1 h at 90 °C, followed by a cure of 2 h at 160 °C.

The densities of the plates were measured. An epoxy density of 1100 kg/m^3 and a silica density of 1800 kg/m^3 were calculated. The volume fraction of silica was calculated from the known weight fractions using the measured densities.

2.2. Glass transition temperatures

The glass transition temperature, T_g, of the various polymers was measured using differential scanning calorimetry. The sample was heated to 175 °C at a rate of 10 °C/min, and then cooled to 0 °C. The sample was then heated again to 175 °C, and the results quoted are from this second heating run.

Dynamic mechanical thermal analysis (DMTA) was performed by testing bars 48 × 3 × 2 mm in size in the three-point-bending mode at 1 Hz. The storage modulus, loss modulus and loss factor, tan δ, were calculated as a function of temperature, over a range from −40 to 175 °C. The glass transition temperature, T_g, was also determined, and was taken to be the temperature at which the peak value of tan δ occurred.

2.3. Mechanical properties

Tensile dumbbell specimens were machined from the plates. These were tested at a displacement rate of 1 mm/min and a test temperature of 21 °C, according to the ISO standard test method [21,22]. The strain in the gauge length was measured using a clip-on extensometer, and the Young's modulus, E, was calculated.

2.4. Fracture testing

The single-edge notch bend (SENB) test was used to determine the fracture toughness, K_{Ic}, at the onset of crack growth of the polymers. Specimens were machined from the sheets, and the fracture toughness was determined according to the relevant ISO standard [23], using a displacement rate of 1 mm/min and a test temperature of 21 °C. Four replicate specimens were tested for each blend composition. The machined notch was sharpened by drawing a razor blade across the notch tip before testing. All the specimens failed by unstable crack growth, and hence only a single initiation value of the fracture toughness was obtained from each specimen. The coefficient of variation in the values of K_{Ic} was ±15%. The value of the fracture energy, G_{Ic}, was calculated from knowledge of the values of K_{Ic} and E, using the relationship:

$$G_{Ic} = \frac{K_{Ic}^2}{E}\left(1 - \nu^2\right) \quad (1)$$

where E is the modulus of elasticity obtained from the tensile tests, and ν is the Poisson's ratio of the polymer, taken to be 0.35 [24].

2.5. Microscopy

The fracture surfaces of the specimens were investigated using scanning electron microscopy (SEM). A JEOL 'JSM-5300' scanning microscope was used, and all specimens were coated with a thin layer of sputtered gold before analysis to prevent charging. An acceleration voltage of 20 kV was used.

High resolution SEM was performed on the fracture surfaces with an electron microscope equipped with a field emission gun (FEG-SEM). The instrument used was a 'Leo 1525' from Carl Zeiss equipped with a 'Gemini' column. Typically, the acceleration voltage was set at 5 kV. All specimens were coated with an approximately 5 nm thick layer of gold or platinum before analysis.

Thin sections, approximately 60–80 nm thick, of the blends were cryo-microtomed (at −50 °C) for subsequent examination using transmission electron microscopy (TEM). The TEM was performed using a JEOL 'JEM-2000FX II' electron microscope at an acceleration voltage of 200 kV.

Atomic force microscopy (AFM) studies were undertaken using a 'MultiMode' scanning probe microscope from Veeco equipped with a 'J' scanner and a 'NanoScope IV' controller. A smooth surface was first prepared by cutting samples on a cryo-ultramicrotome at temperatures down to −100 °C. The scans were performed in tapping mode using silicon probes, and both height and phase images were recorded.

2.6. Surface roughness

Surface roughness measurements of the fracture surfaces were performed using a 'Form Talysurf Series 2'. A sharp stylus with a tip radius of 2.5 μm, attached to a cantilever, was drawn across the surface at a constant speed for a set distance. Five measurements with a traverse length of 4 mm were performed perpendicular to the direction of the crack growth. The average roughness, R_a, of the line profiles was calculated.

2.7. Microstructure

Microscopy of the unmodified epoxy polymer showed that a homogeneous thermoset was formed. For the nanosilica-modified materials, atomic force and transmission electron micrographs both showed that there was no agglomeration of the nanosilica particles, even at higher volume fractions of nanosilica. Instead, the particles are well-dispersed throughout the epoxy, as shown in Figs. 1 and 2. These images confirm that the nanoparticles are approximately 20 nm in diameter. Note that the TEM slice shown in Fig. 2 is approximately 100 nm thick, and hence the apparent volume fraction of particles is higher than the true volume fraction.

3. Results

3.1. Glass transition temperatures

Dynamic mechanical thermal analysis (DMTA) was used to determine the storage modulus, G', and the glass transition temperature, T_g, of the formulations used. A T_g of 153 °C was measured for the unmodified epoxy polymer, as shown in Table 1 and Fig. 3. Addition of the nanosilica did not significantly affect the measured glass transition temperature, and all values lay within the range 152 ± 2 °C. The glass transition temperatures measured using differential scanning calorimetry also showed no significant effect of the addition of nanosilica,

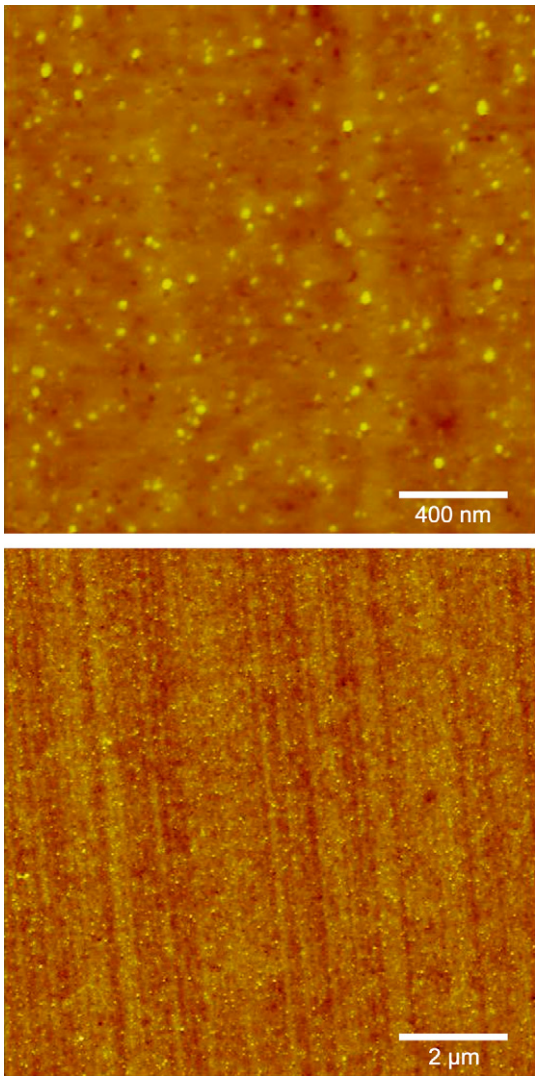

Fig. 1. Atomic force micrographs (height image) of the epoxy polymer containing 9.6 vol% nanosilica.

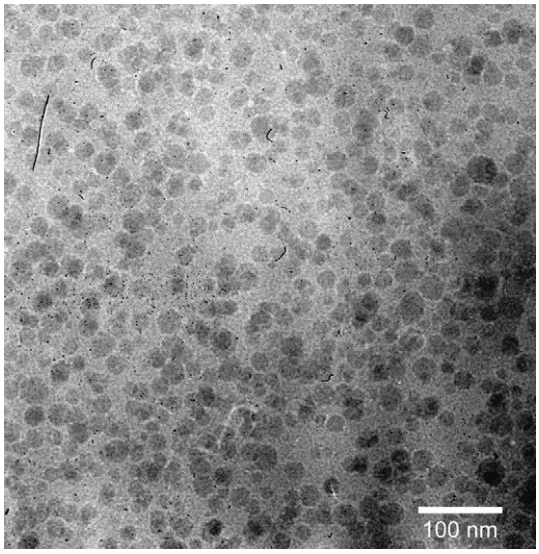

Fig. 2. Transmission electron micrograph of the epoxy polymer containing 9.6 vol% nanosilica.

Table 1
Glass transition temperatures, modulus and fracture properties of the anhydride-cured epoxy polymer containing nanosilica particles

Nanosilica content (wt%)	Nanosilica content (vol%)	T_g (°C) DSC	T_g (°C) DMTA	E (GPa)	K_{Ic} (MN m$^{-3/2}$)	G_{Ic} (J/m^2)
0	0	143	153	2.96	0.59	103
4.1	2.5	137	152	3.20	1.03	291
7.8	4.9	136	154	3.42	1.17	352
11.1	7.1	141	151	3.57	1.18	343
14.8	9.6	138	152	3.60	1.29	406
20.2	13.4	138	150	3.85	1.42	461

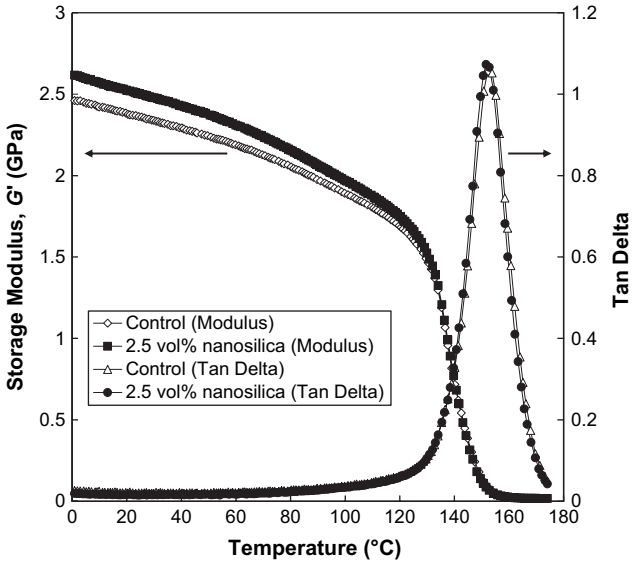

Fig. 3. Dynamic mechanical thermal analysis data, showing flexural modulus and loss factor (tan δ), measured at 1 Hz, versus temperature for unmodified epoxy polymer and epoxy polymer with 2.5 vol% nanosilica.

with T_g values of 140 ± 3 °C being measured. (Note that DMTA gave somewhat higher T_g values than those obtained using differential scanning calorimetry, as has been observed previously when comparing these techniques, e.g. by Johnsen et al. [25].) The modulus determined from the DMTA tests gave a similar trend to that observed using the tensile tests discussed below.

3.2. Tensile modulus

A tensile modulus of 2.96 GPa was measured for the unmodified epoxy polymer. The measured modulus was found to increase with the nanosilica content, see Fig. 4. The increase in modulus is expected because the modulus of silica, $E = 70$ GPa [26,27], is much greater than that of the epoxy matrix. A maximum modulus of 3.85 GPa was measured, for the epoxy polymer with 13.4 vol% of nanosilica. The measured moduli can be compared to theoretical predictions.

There are many theoretical models that may be used to predict the moduli of particle-modified polymers, e.g. [28–30]. The most commonly used models are the rule of mixtures, the Halpin–Tsai and the Mori–Tanaka relationships. Other

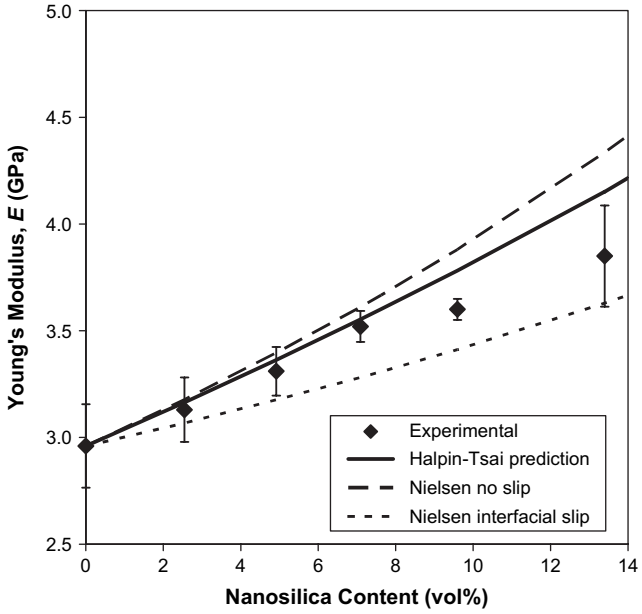

Fig. 4. Tensile modulus versus nanosilica content. Points are experimental data, and solid line is the prediction using the Halpin–Tsai model. The dashed lines are predictions using the McGee and McCullough form of the Lewis–Nielsen model for no slippage at the particle-matrix interface ($k_E = 2.167$) and for interfacial slippage ($k_E = 0.867$) for non-agglomerated spheres in a matrix with $\nu = 0.35$.

models are summarised in review papers by Ahmed and Jones [31] and by Nielsen and Landel [32]. Note that these models make a number of assumptions. They assume that the matrix and the particles are linear-elastic, isotropic and that there is perfect bonding between the particles and the matrix. They also assume that the particles are (where applicable) uniform in their aspect ratio and perfectly aligned with the applied load. Many models also ignore any agglomeration and particle–particle interactions.

The rule of mixtures and the modified rule of mixtures have generally been found to give poor predictions [33], and they also give poor predictions when compared to the present experimental data. They will not be considered further. The Mori–Tanaka model is also frequently used for predicting the modulus of particle-modified polymers [34,35]. Here the particles are treated as ellipsoidal (either fibre-like or plate-like) with a constant aspect ratio, and are assumed to be aligned. However, this model works best for relatively high aspect ratios, as when the aspect ratio approaches unity the model predicts a negligible reinforcing effect, and hence is not suitable for use in the present work.

The Halpin–Tsai model comes from work by Halpin and co-workers [30,36], and gives the modulus of the material as a function of the modulus of the matrix polymer, E_m, and of the filler particles, E_f, and also as a function of the aspect ratio by the inclusion of a shape factor. The predicted composite modulus is

$$E_c = \frac{1 + \zeta \eta V_f}{1 - \eta V_f} E_m \tag{2}$$

where ζ is the shape factor, V_f is the volume fraction of particles, and

$$\eta = \left(\frac{E_f}{E_m} - 1\right) \Big/ \left(\frac{E_f}{E_m} + \zeta\right) \tag{3}$$

Halpin and Tsai noted that the value of ζ must lie between zero and infinity. Indeed, if $\zeta = \infty$ then Eq. (2) reduces to the rule of mixtures, and if $\zeta = 0$ then it reduces to the transverse rule of mixtures. They suggested that the value of ζ correlated with the geometry of the reinforcing phase, especially with the aspect ratio (w/t) of the particles, where w is the length of the particle and t is its thickness. By comparison of the predictions with the results of a finite-element analysis, Halpin and Kardos [37] suggested that a shape factor of $\zeta = 2w/t$ is used for calculating the modulus of a polymer with the particles aligned with the loading direction. They recommended using $\zeta = 2$ for the modulus perpendicular to the loading direction. For the spherical particles used in the present work the aspect ratio is unity, and hence $\zeta = 2$ will be used.

The predictions are shown with the experimental data in Fig. 4. This figure shows that the modulus is expected to increase with the volume fraction of nanosilica [38], and that the agreement between the predictions and experimental data is reasonable. However, the measured moduli generally lie slightly below the predicted relationship. This is a common observation, as the model assumes that there is perfect bonding between the particles and the matrix, which is normally not the case. This effect can be considered further using the Lewis–Nielsen model [39] and the work of McGee and McCullough [40]. The authors showed that the composite modulus can be predicted using:

$$E_c = \frac{1 + (k_E - 1)\beta V_f}{1 - \beta\mu V_f} E_m \tag{4}$$

where k_E is the generalised Einstein coefficient, and β and μ are constants. The constant β takes into account the relative modulus of the particles and the matrix, and is given by

$$\beta = \left(\frac{E_f}{E_m} - 1\right) \Big/ \left(\frac{E_f}{E_m} + (k_E - 1)\right) \tag{5}$$

The value of μ depends on the maximum volume fraction of particles, V_{max}, and can be calculated from

$$\mu = 1 + \frac{(1 - V_f)}{V_{max}}\left[V_{max}V_f + (1 - V_{max})(1 - V_f)\right] \tag{6}$$

Values of V_{max} have been tabulated by Nielsen and Landel [32] for a range of particle shapes and types of packing. The micrographs shown in the present work indicate that the particles appear non-agglomerated and randomly arranged. For random close packing, non-agglomerated spheres, Nielsen and Landel quote a value of $V_{max} = 0.632$. This value will be used in the modulus predictions.

The value of k_E varies with the degree of matrix to particle adhesion. For a matrix with a Poisson's ratio of 0.5 containing dispersed spheres, $k_E = 2.5$ if there is no slippage at the interface, and $k_E = 1.0$ if there is slippage [32]. Nielsen [41] has shown that the value of k_E is reduced when the Poisson's ratio of the matrix is lower than 0.5. In the present work $\nu = 0.35$, so values of k_E are reduced by a factor of 0.867. Hence, $k_E = 2.167$ if there is no slippage and $k_E = 0.867$ if there is slippage. The predictions for these two cases are shown in Fig. 4. It can be seen that reducing the adhesion, and hence the value of k_E, reduces the predicted modulus. The Lewis–Nielsen predictions bracket the experimental data, and indicate that there is likely to be imperfect adhesion between the particles and the matrix.

An alternative explanation for the relatively poor agreement being observed between the Halpin–Tsai model and the experimental data is the agglomeration of the particles. The values of the maximum volume fraction of particles and the Einstein coefficient in the Lewis–Nielsen model take into account the degree of dispersion of particles. For example, for random close-packed agglomerated particles, $V_{max} = 0.37$, and $k_E = 6.76 \times 0.867 = 5.86$ [32]. Substitution of these values into the equations above gives predictions which are higher than the Lewis–Nielsen prediction with no slippage, as shown in Fig. 4, and hence the agreement between the experimental data and the modified model becomes worse. In addition, the micrographs of the materials used to show no agglomeration of the silica nanoparticles, and hence it seems unlikely that agglomeration is responsible for the relatively poor agreement between the Halpin–Tsai model and the experimental data.

3.3. Fracture toughness and fracture energy

A mean fracture toughness, K_{Ic}, of 0.59 MN m$^{-3/2}$ was measured for the unmodified epoxy polymer. The measured toughness was increased by the addition of nanosilica, and a maximum K_{Ic} of 1.42 MN m$^{-3/2}$ was measured for the polymer with 13.4 vol% nanosilica, see Table 1. The fracture energy, G_{Ic}, was calculated for each formulation via Eq. (1), using the modulus measured by tensile testing. These data are shown in Fig. 5 and Table 1. The fracture energy increases steadily with the nanosilica content, see Fig. 5.

3.4. Fracture surfaces

The fracture surface of the unmodified epoxy polymer is shown in Fig. 6a, where the direction of crack propagation is from left to right. The fracture surface is relatively smooth and glassy, which is typical of a brittle thermosetting polymer [42], and shows that no large-scale plastic deformation has occurred during fracture. These observations agree well with the low measured toughness of the material, where $K_{Ic} =$ 0.59 MN m$^{-3/2}$. In addition, there are apparent steps and changes of the level of the crack which can be observed in Fig. 6a. These features are feather markings, which are caused by the crack forking due to the excess of energy associated with the relatively fast crack growth. This repeated forking and the multi-planar nature of the surface are ways of absorbing this excess energy in a very brittle material [43].

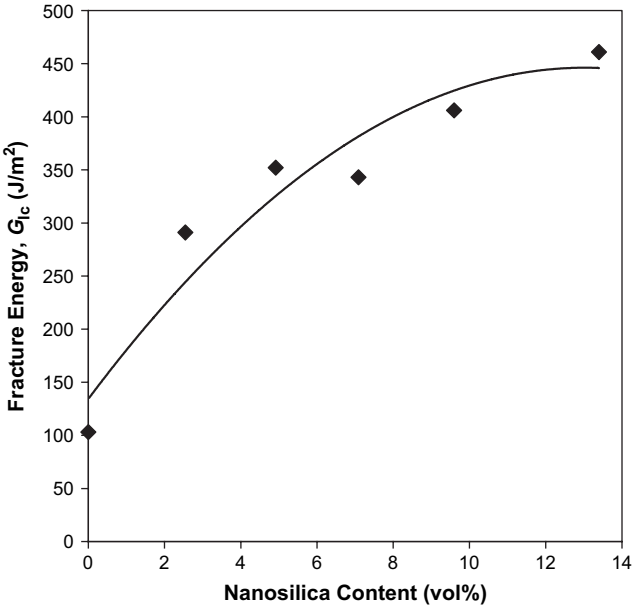

Fig. 5. Fracture energy, calculated using Eq. (1), versus nanosilica content.

The fracture surface of the nanosilica-modified materials showed similar features to those of the unmodified epoxy polymer, as shown in Fig. 6b and c. Crack forking and feather markings are observed, and the fracture surfaces have a brittle appearance. However, the addition of nanosilica did not give an apparent increase in the roughness observed by scanning electron microscopy, unlike for micrometre-sized particles, e.g. [33]. This aspect is discussed in more detail below.

3.5. Toughening micromechanisms

Many authors have observed that the addition of particles to a brittle material increases the measured fracture energy. Huang and Kinloch postulated that the fracture energy of a particle-modified polymer may be expressed [44] as:

$$G_{Ic} = G_{Icu} + \Psi \tag{7}$$

where G_{Icu} represents the fracture energy of the unmodified epoxy, and Ψ represents the overall toughening contributions.

These toughening contributions have been ascribed to a range of processes. They can be broadly categorised as on-plane processes (such as crack pinning or bowing and crack deflection) or off-plane processes (such as debonding and plastic void growth). The following discussion considers these processes in more detail, and uses analytical models to predict the toughening contributions from these processes.

3.5.1. Crack pinning

A crack pinning mechanism has been invoked for micrometre-sized glass particles [10,45,46], and also for nanoparticles [18]. This draws parallels to the impediment of the movement of dislocations through metals by particles (dispersion hardening), e.g. [47], where the dislocation bows between particles, increasing its length. As the energy of a dislocation is proportional to its length, additional energy input is therefore required. Reducing the spacing between the particles and their size will increase the strengthening (toughening) effect [27].

Crack pinning is identified by the presence of bowing lines on the fracture surface. Lange [48] identified pinning by the bowed shape of the crack front in perfectly brittle materials, e.g. glass and magnesium oxide, and Green et al. [49] measured the shape of the bowed crack at breakaway from the pinning particles in glass containing 132 μm diameter nickel particles. Kinloch et al. [45] also observed bowing lines using an epoxy matrix containing 50 μm diameter spherical glass particles.

In these cases, crack pinning occurred when the particles were larger than the crack-opening displacement. To see if a pinning argument is reasonable for nanoparticles, the crack-opening displacement can be calculated and compared to the particle size. The plastic zone ahead of the crack tip can be modelled as a line-zone using the Irwin analysis. Under plane-strain conditions, the crack-opening displacement, δ_{tc}, can be calculated using the relationship [50]:

$$\delta_{tc} = \frac{K_{Ic}^2}{E\sigma_y}\left(1-\nu^2\right) = \frac{G_{Ic}}{\sigma_y} \tag{8}$$

where σ_y is the yield stress of the matrix.

For the unmodified epoxy polymer, using the data in Tables 1 and 2, the value of the crack-opening displacement is 1.7 μm. For the maximum toughness measured in the present work, using the 13.4 vol% nanosilica formulation, a value of $\delta_{tc} = 7.5$ μm is calculated, as shown in Table 3. The crack tip is shown schematically in Fig. 7, which shows the relative size of the nanoparticles and the crack-opening displacement. From this figure, it is clear that particles which are so much smaller than the crack-opening displacement are unlikely to cause crack pinning. Indeed, the crack pinning and bowing analysis by Green et al. [51] require that the particles are much larger than the plastic zone size. This is not the case in the present work, as the nanosilica particles have a mean particle size of about 20 nm, whereas the diameter of the plastic zone varies from 5 to 29 μm, as shown in Table 3.

By comparison, where crack pinning has been observed, the particle diameter is much larger than the crack-opening displacement. Kinloch et al. [45] quoted $\delta_{tc} = 1.8$ μm at room temperature while the mean particle diameter was 50 μm, using an epoxy matrix with glass particles. In this case the diameter of the smallest plastic zone was about 35 μm. Similarly, Green et al. [49] demonstrated pinning with 132 μm diameter particles, but $\delta_{tc} = 0.3$ μm and the diameter of the plastic zone was less than 60 μm (conservative estimates calculated assuming that the yield stress is equal to the quoted fracture stress). Others [10,13,45,46] have invoked pinning though the lack of microscopic evidence makes it difficult to establish whether pinning really occurred. Norman and Robertson [52] observed no bowing lines on the fracture surfaces and discounted crack pinning, finding that off-plane processes dominated the toughening effect.

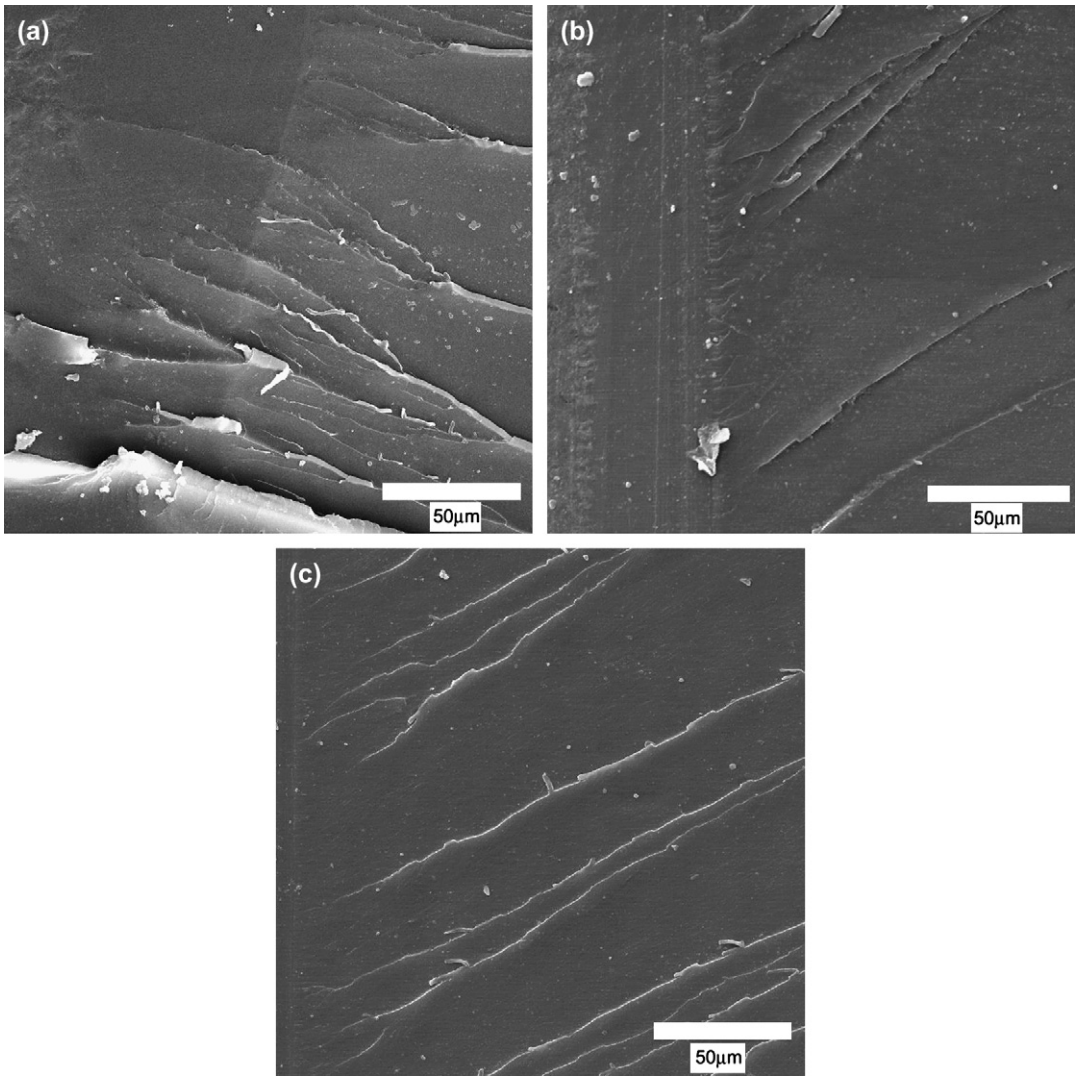

Fig. 6. Scanning electron micrographs of fracture surfaces, showing the precrack towards the left of the image, for (a) unmodified epoxy polymer, (b) epoxy polymer with 2.5 vol% nanosilica, and (c) epoxy polymer with 13.4 vol% nanosilica. (Crack propagation is from left to right.)

As the nanosilica particles are so much smaller than the crack-opening displacement they are unlikely to cause crack pinning, and this conclusion is supported by the theory. The absence of bowed crack front markings on the fracture surfaces in the present work, and that by Zhang et al. [18], indicates that crack pinning is unlikely to be responsible for the observed increase in toughness.

Table 2
Material properties of the unmodified epoxy polymer, and constants used for calculation of the fracture energy, G_{Ic}, and for the contribution to the increase in fracture energy from the plastic void growth mechanism, ΔG_v

Property	Symbol	Ref.	Units	Value
Fracture toughness	K_{Ic}	1	MN m$^{-3/2}$	0.59
Modulus	E_m	1	GPa	2.96
Poisson's ratio	ν	[24]	–	0.35
Tensile yield stress	σ_y	1	MPa	61.1
Compressive yield stress	σ_{yc}	1	MPa	77.3
von Mises pressure sensitivity	μ_m	[65]	–	0.2
Max. stress concentration factor	K_{vm}	[65]	–	2.22

1: Measured in the present work.

3.5.2. Crack deflection

The toughening effect could be due to crack deflection occurring, where the crack front tilts and twists when it encounters the particles and hence passes around them [42,53]. This causes an increase in the total fracture surface area and also causes the crack to grow locally under mixed-mode I/II conditions. The former toughening effect can be evaluated by (i) comparing the measured fracture toughness with the surface

Table 3
Theoretical values of the crack-opening displacement and the plastic zone size using the Irwin model, calculated using Eqs. (8) and (11)

Nanosilica content (wt%)	Nanosilica content (vol%)	Crack-opening displacement δ_{tc} (μm)	Radius of a circular plastic zone r_y (μm)
0	0	1.7	4.9
4.1	2.5	4.8	15
7.8	4.9	5.7	19
11.1	7.1	5.6	20
14.8	9.6	6.6	24
20.2	13.4	7.5	29

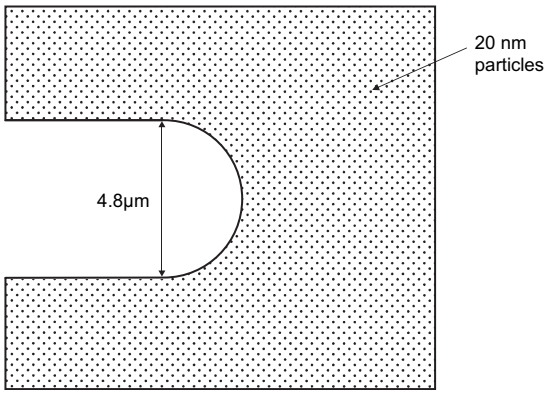

Fig. 7. Schematic showing crack tip, with calculated crack-opening displacement (from Eq. (8)) and nanoparticles for the epoxy polymer containing approximately 2.5 vol% nanosilica.

roughness, and (ii) the latter toughening effect can be evaluated using the analysis by Faber and Evans [53].

Work by Arakawa and Takahashi [54], as reported by Hull [55,56], showed that the toughening effect due to an increase in the true fracture surface area gives a linear relationship between the surface roughness and the overall toughening contribution, Ψ [54]. In the present work, the average surface roughness, R_a, of the fracture surfaces was measured. The average roughness of the unmodified epoxy polymer was relatively low, an R_a value of 0.04 μm being measured, which is typical for an unmodified epoxy polymer, e.g. [33]. The roughness generally increased with an increasing concentration of nanosilica, from a minimum of $R_a = 0.03$ μm at 2.5 vol% nanosilica to a maximum of $R_a = 0.15$ μm at a concentration of 13.4 vol% nanosilica. These data are shown in Fig. 8, where the measured roughness is plotted against the overall toughening contribution, Ψ, from the presence of the nanosilica. These do not show a linear relationship, and hence it appears that

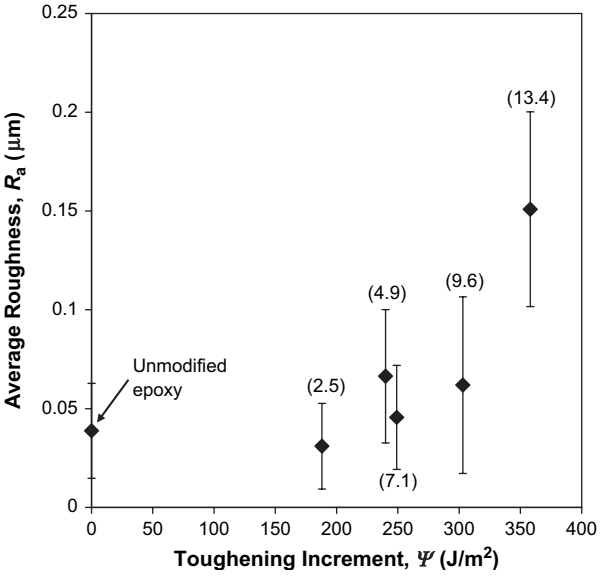

Fig. 8. Mean roughness of the fracture surfaces versus measured toughening increment, Ψ. The volume fractions of nanosilica are shown in parentheses, error bars are 1 standard deviation.

increases in the true (i.e. local) fracture surface area are not solely responsible for the increases in the toughness.

The measured fracture energies may also be compared to predictions by Faber and Evans [53], which consider that crack deflection causes the crack to grow locally under mixed-mode I/II conditions. This analysis uses the shape of the particles, which is spherical in this case, and their volume fraction. For example, the Faber and Evans model predicts that the fracture energy for a volume fraction of 2.5% of silica spheres will be 1.2 times that of the unmodified epoxy. The G_{Ic} of the pure epoxy is 103 J/m^2 and thus the predicted value of G_{Ic} from employing the Faber and Evans model is 120 J/m^2. However, the measured fracture energy of 291 J/m^2 is significantly higher than this predicted value. The Faber and Evans model consistently underpredicts the fracture energy, and this suggests that this mechanism is unlikely to fully explain the increased toughness.

In addition, Fig. 7 shows that the nanoparticles are so much smaller than the crack-opening displacement that they are unlikely to cause the crack to deflect. Indeed, Evans states that the equations can only be used provided that the obstacle dimension is larger than the plastic zone [57], which is not the case in the present work, as discussed above. This and the relatively poor agreement with the crack deflection models indicate that crack deflection is unlikely to fully explain the observed toughening effect.

3.5.3. Immobilised polymer

Another mechanism that has been proposed [18,58] is the formation of an interphase or immobilised layer of polymer around the particles. Because the interparticle distance for nanocomposites is so small, it is suggested that due to the proximity of the particles this interphase may be present throughout the entire polymer matrix. The formation of an immobilised layer of polymer around particles has been observed for various systems. Using absorption studies, the bound layer thickness is typically 1–5 nm for carbon black-elastomer systems [59], and values of 10–20 nm have been reported for rutile (TiO_2) filled polyethylene [60]. Viscometric studies generally give larger thicknesses [59], in the order of tens of nanometres, and values as high as 1.4 μm have been reported for PMMA with glass particles [61].

Thermal analysis has also been used. Work by Gerard et al. [62] comparing treated and untreated glass particles in an epoxy matrix, as reported by Rothon and Hancock [59], showed that uncoated particles reduce the mobility of the polymer. However, when the particles were coated with a rubbery interlayer the effect was largely absent. In addition, immobilisation of the polymer would be expected to increase T_g of the epoxy [62], and/or to broaden the dynamic mechanical peak, see Iisaka and Shibayama [63] for example. However, Fig. 3 shows that both the width and position of the tan δ peak measured using DMTA are unaffected. The same is true for the other DMTA data, as confirmed by the T_g values which are summarised in Table 1.

Hence it can be concluded that there is no evidence for a toughening mechanism which involves the formation of an immobilised layer of polymer around the nanosilica particles.

3.5.4. Plastic void growth

The toughening mechanisms associated with micrometre-sized particles have frequently been shown to be due to debonding of the particles followed by plastic void growth, e.g. [12,13,42]. Indeed, Kinloch and Taylor [42] have also demonstrated that the voids around particles closed-up when the epoxy polymer was heated above its T_g and allowed to relax. The debonding process is generally considered to absorb little energy compared to the plastic deformation of the matrix. However, debonding is essential because this reduces the constraint at the crack tip and hence allows the matrix to deform plastically via a void growth mechanism.

High resolution scanning electron microscopy (FEG-SEM) of a fracture surface of the polymer containing 9.6 vol% nanosilica, see Fig. 9, showed the presence of voids around several of the nanoparticles. This shows that plastic void growth of the epoxy matrix, initiated by debonding of the nanoparticles, has occurred. The diameter of these voids is typically 30 nm. These voids were also observed in the fracture surfaces of samples with different contents of nanosilica. Although the samples are coated to prevent charging in the electron microscope, the voids are not an artefact of the coating as they could not be observed on a coated fracture surface of the pure epoxy polymer, see Fig. 10. Also, the nanosilica-modified samples appeared similar whether they were coated with platinum or gold.

In addition, similar voids were observed by AFM of uncoated fracture surfaces, see Fig. 11. However, the apparent diameter of the nanoparticle in the void highlighted in Fig. 11 is 30 nm, as shown in Fig. 12, whereas transmission electron microscopy has shown that the mean particle size is actually around 20 nm. This discrepancy is due to the tip-broadening effect when the AFM is used to identify such small features. As the tip radius of the AFM probe is about 10 nm, this makes

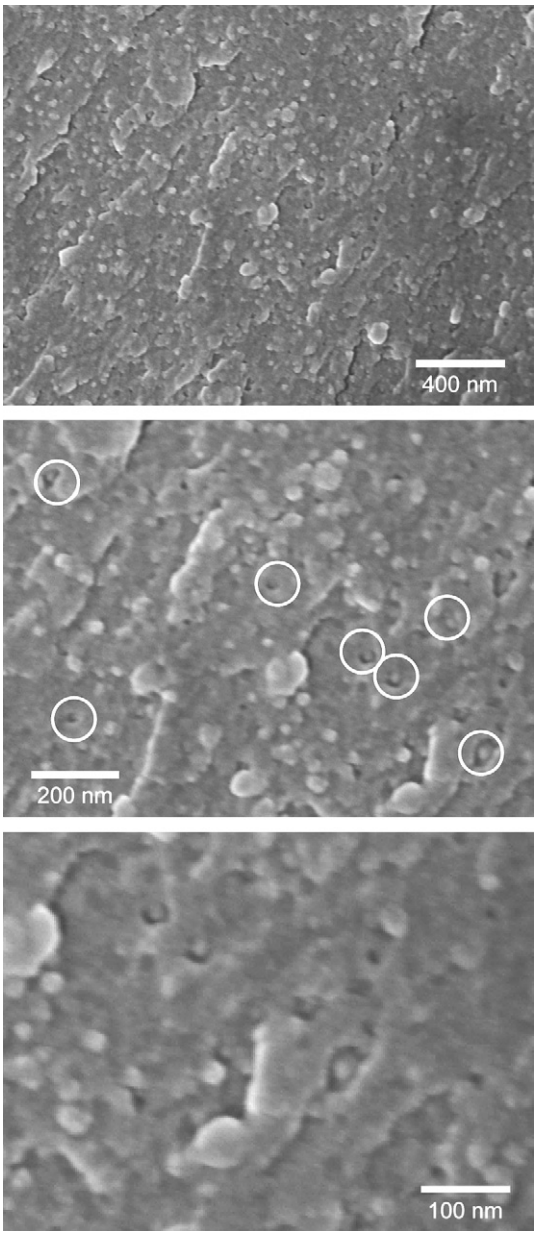

Fig. 9. Scanning electron micrographs (FEG-SEM) of the fracture surface of the epoxy polymer containing 9.6 vol% nanosilica. (Voids with nanoparticles are circled in the central image.)

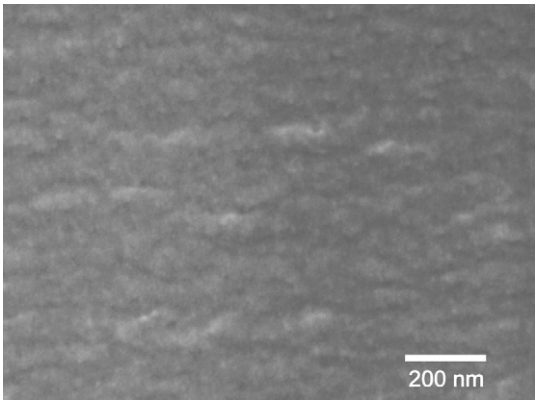

Fig. 10. Scanning electron micrograph (FEG-SEM) of the fracture surface of the unmodified epoxy polymer.

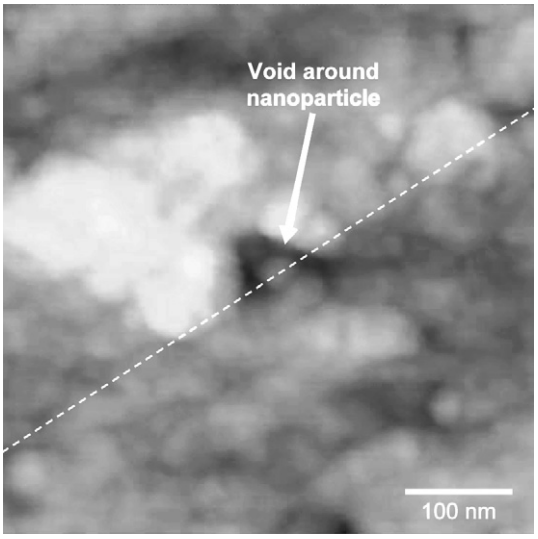

Fig. 11. Atomic force micrograph (height image) of a fracture surface of the epoxy polymer containing 9.6 vol% nanosilica.

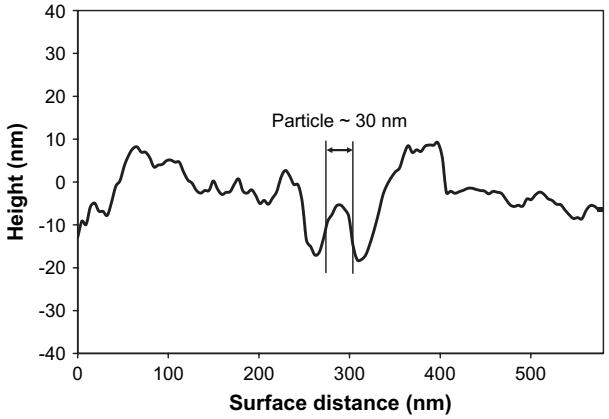

Fig. 12. Surface profile of the line drawn across the nanosilica particle and void in Fig. 11.

features that are protruding out of a surface appear larger than their true size in the micrographs. The void diameter in this case is about 70 nm, and it would appear that AFM can only be reliably used to detect the largest voids.

Voids with no nanoparticles were also observed with FEG-SEM. Here the particles associated with these voids will be situated in the opposite fracture surface, or have fallen out of the surface completely during fracture, as is commonly observed with micrometre-sized particles [42]. (It should be noted that the diameters of most of these holes are less than those discussed above, as the matrix is unlikely to fail across the widest point of the void. Further, the coating, which is 5 nm thick, will partially fill the voids, and hence the observed size may be smaller than the true (uncoated) diameter.)

3.5.5. Modelling of the contribution from the plastic void growth mechanism

To confirm whether the observed debonding and plastic void growth which occur for the nanoparticle-modified epoxy could be responsible for the toughening effect, the increase in toughness can be compared to a theoretical model. A suitable model for this is by Huang and Kinloch [44]. This model assumes that the fracture specimens behave in a bulk linear-elastic manner, and that the energy dissipation is localised to a small plastic zone at the crack tip, as observed in the present work.

Huang and Kinloch suggested that the overall toughening contribution, Ψ, was composed of contributions from particle bridging, localised shear banding in the epoxy matrix, and plastic void growth of the epoxy matrix which is initiated by cavitation or debonding of the particulate phase. However, for rigid spherical particles as used in the present work, microscopy has shown that bridging does not occur. Hence the plastic void growth mechanism seems to be by far the dominant toughening micromechanism, and thus the relationship in Eq. (7) may be written as:

$$G_{Ic} \approx G_{Icu} + \Delta G_v \tag{9}$$

where ΔG_v is the contribution to the increase in fracture energy from plastic void growth of the epoxy matrix. For simplicity, we will initially assume that the adhesion between the silica and epoxy polymer phases is relatively poor, and hence debonding will not contribute to the toughening effect. The contribution to the increase in fracture energy from the plastic void growth mechanism, ΔG_v, is given [44] by

$$\Delta G_v = \left(1 - \mu_m^2/3\right)\left(V_v - V_f\right)\sigma_{yc} r_{yu} K_{vm}^2 \tag{10}$$

where μ_m is a material constant, V_v is the volume fraction of voids, V_f is the volume fraction of particles, σ_{yc} is the compressive yield stress of the unmodified epoxy polymer, r_{yu} is the radius of the plastic zone of the unmodified epoxy polymer, and K_{vm} is the maximum stress concentration factor of the von Mises stress in the plastic matrix. The value of μ_m, which describes the pressure sensitivity of the material in the von Mises yield criterion, has been reported [64] to be between 0.175 and 0.225, and is normally taken to be 0.2, as reported in [44]. The material properties for the calculation of ΔG_v are summarised in Table 2. The maximum stress concentration factor, K_{vm}, was found from a finite-element analysis [65] to be 2.22 around a void in an epoxy matrix.

The size of the plastic zone ahead of the crack tip can be calculated assuming linear-elastic fracture-mechanics (LEFM) behaviour. Under plane-strain conditions and assuming that the zone is circular [50] as proposed by Irwin, the radius of the plastic zone, r_y, is given by

$$r_y = \frac{1}{6\pi}\left(\frac{K_{Ic}}{\sigma_y}\right)^2 \tag{11}$$

In the present work, for the unmodified epoxy polymer $K_{Ic} = 0.59\ \mathrm{MN\,m^{-3/2}}$, $\sigma_y = 61.1$ MPa and hence $r_{yu} = 5\ \mu\mathrm{m}$.

Now, Eq. (10) requires knowledge of the volume fraction of voids and it is difficult to measure this parameter accurately from the micrographs, as it is difficult to identify all the voids due to the resolution of the microscopes used. Nevertheless, a mean void diameter can be calculated from the features which are clearly voids, see Fig. 9 for example. Analysis of micrographs of the polymer with 9.6 vol% nanosilica gave a mean void diameter of 30 nm. Micrographs of the formulation containing 2.5 vol% nanosilica indicated an average void diameter of just below 30 nm. However, some voids up to 50 nm in diameter are observed in all formulations where micrographs from FEG-SEM analysis are available.

The predicted toughening increment, Ψ, was calculated using Eqs. (7), (10) and (11), assuming (a) that the measured toughening increment is entirely caused by plastic void growth (i.e. $\Psi = \Delta G_v$), and (b) that all of the particles initiate the growth of voids which have a final diameter of 30 nm. For the epoxy with 9.6 vol% of nanosilica, the measured toughening increment is 303 J/m^2 and the predicted toughening increment is 394 J/m^2. The toughening increment can also be predicted for the other formulations, for which FEG-SEM images are not available, assuming that the average void diameter is constant and that all of the particles initiate void growth. The results are shown in Table 4.

Table 4
Measured and predicted toughening increments

Nanosilica content (wt%)	Nanosilica content (vol%)	Toughening increment, Ψ (J/m^2)	
		Measured	Predicted
4.1	2.5	188	107
7.8	4.9	249	209
11.1	7.1	240	297
14.8	9.6	303	394
20.2	13.4	358	540

Predicted values calculated using Eqs. (7) and (10), assuming that $\Psi = \Delta G_v$. (Note $G_{Icu} = 103$ J/m^2.)

Considering the assumptions made in the above quantitative modelling calculations, then firstly, it is highly unlikely that all of the particles will debond and initiate void growth. Indeed, from the FEG-SEM images of the fracture surfaces in Fig. 9 it can be seen that not all of the nanosilica particles seem to initiate void growth. The difficulty of quantifying the number of debonded particles, when considering the present nanosilica particles, has been discussed above and has been reported by van Hartingsveldt and van Aartsen [66] who studied the debonding of glass particles with a diameter of 20–50 μm in a polyamide matrix. They clearly demonstrated that only a fraction of the particles debonded, but that this fraction could be as high as about 0.8–0.9. Further, such a value was attained at levels of applied strain which are relatively low compared to those which exist in the region of the crack tip, as is being considered in the present work. Also, the present nanosilica particles do possess a very narrow distribution of particle size. Thus, they would be expected to possess an almost constant value of the applied stress needed to debond them [67,68], and hence might be expected to exhibit a relatively high fraction of particles which show a similar behaviour. (Although, previous work [67,68] has suggested that, for a given level of interfacial adhesion, the nanosilica particles should require a relatively high level of debonding stress compared to glass particles which are many micrometres in diameter.) Thus, on balance, it appears not unreasonable to assume that most of the nanosilica particles will debond and initiate plastic void growth in the epoxy matrix. However, clearly, if only a fraction of the particles initiates void growth, or if only partial debonding occurs, then the predicted toughening increments would be reduced compared to the values shown in Table 4.

Secondly, for simplicity, it has been assumed that the adhesion between the silica and epoxy phases was poor. If this is not the case, then the energy absorbed by the debonding process will also contribute to the toughening effect. Thirdly, the presence of nanoparticles in the ligaments between the debonded nanoparticles will increase the stiffness of the plastically-deforming ligaments, and hence may be expected to increase the strain-energy density absorbed by the ligaments during their plastic deformation. Indeed, the data from tensile tests show that the strain to failure is unaffected by the addition of nanoparticles, but the modulus and the strength are increased. Hence, the strain-energy density at fracture (in a tensile test) of the nanosilica-modified epoxy polymer is greater than that of the pure epoxy polymer. Clearly, both of these effects would tend to lead to the experimentally measured values of G_{Ic} being greater than the predicted values. Hence, these effects would offset the above effect of not all of the particles debonding. Nevertheless, there is no direct evidence for these effects being of significance and, for the present, will not be considered further.

In summary, considering the simplifying assumptions made, the agreement between the measured and the predicted toughening increments is very reasonable. The predicted values are somewhat larger than the measured values for the high nanosilica contents, but the predicted values agree very well with the experimental data for the lower nanosilica contents. This confirms that plastic void growth of the epoxy matrix, initiated by a void being formed by debonding of the nanosilica, can indeed produce the major increases in the values of the fracture energy, G_{Ic}, recorded in the present work.

4. Conclusions

An epoxy resin cured with an anhydride has been used. This was modified by the addition of silica nanoparticles, manufactured using a sol–gel process, which were 20 nm in diameter. These particles were well-dispersed through the epoxy matrix with no agglomeration observed using transmission electron and atomic force microscopies. The addition of the nanoparticles did not affect the glass transition temperature; the T_gs of the unmodified and nanoparticle-modified epoxy polymers were measured to be in the range of 140 ± 4 °C using differential scanning calorimetry. Dynamic mechanical thermal analysis confirmed this observation. The addition of nanoparticles increased the modulus of the epoxy polymer as expected. The measured moduli were compared to theoretical values, calculated using the Halpin–Tsai and Lewis–Nielsen models, and good agreement was found.

The fracture toughness of the polymers was measured, and a K_{Ic} of 0.59 MN m$^{-3/2}$ was recorded for the unmodified epoxy. Addition of the nanoparticles increased the fracture toughness, a maximum value of 1.42 MN m$^{-3/2}$ being measured for the epoxy polymer with 13.4 vol% of nanoparticles. These values were converted to fracture energies, G_{Ic}, using the measured modulus. The unmodified epoxy polymer gave $G_{Ic} = 103$ J/m^2, and a maximum fracture energy of 460 J/m^2 was calculated. Hence there is a significant toughening effect due to the addition of the silica nanoparticles.

The toughening mechanisms for particle-modified epoxy polymers reported in the literature were reviewed. The constant T_g values discount the immobilised polymer mechanism, and the lack of pinning marks on the fracture surfaces indicates that crack pinning is not occurring. Crack deflection was discounted by a lack of correlation between the measured roughness of the fracture surfaces and the toughening increment. As the silica nanoparticles are so much smaller than the crack-opening displacement, it is unlikely that these on-plane mechanisms are responsible for the toughening effect. Indeed, these theories assume that the particle diameter is much greater than the plastic zone size, which is not the case with nanoparticles.

Observation of the fracture surfaces using scanning electron and atomic force microscopies showed nanoparticles surrounded by voids, providing evidence of debonding of the nanoparticles and subsequent plastic void growth. An analytical model of plastic void growth was used to confirm whether this mechanism could be responsible for the increased toughness. The mean void diameter was measured from the micrographs, and the model was used to predict the toughening increment (compared to the fracture energy of the unmodified epoxy polymer). The predicted values agreed well with the measured values, indicating that debonding of the nanoparticles and subsequent plastic void growth were most likely to be responsible for the increase in toughness that was observed due to the presence of the nanosilica particles.

Acknowledgements

The authors gratefully acknowledge the financial support provided by the Government of Trinidad and Tobago via a studentship for Mr. R.D. Mohammed. Also, they wish to acknowledge the general support from the US Army European Research Office and Nanoresins (formerly Hanse Chemie). They would also like to thank Dr. B.R.K. Blackman, Mr. M.Z. Sanat, Dr. M.G. Ardakani (Imperial College London) and Dr. I.A. Kinloch (University of Manchester) for their assistance with the microscopy.

References

[1] Drake RS, Siebert AR. SAMPE Quart 1975;6(4):11–21.
[2] Kinloch AJ, Shaw SJ, Tod DA, Hunston DL. Polymer 1983;24(October):1341–54.
[3] Kinloch AJ. MRS Bull 2003;28(6):445–8.
[4] Rowe EH, Siebert AR, Drake RS. Mod Plast 1970;47(August):110–7.
[5] Pearson RA, Yee AF. J Mater Sci 1986;21(7):2475–88.
[6] Pascault JP, Williams RJJ. Formulation and characterization of thermoset–thermoplastic blends. In: Paul DR, Bucknall CB, editors. Polymer blends volume 1: formulation. New York, USA: John Wiley & Sons; 1999. p. 379–415.
[7] Bucknall CB, Partridge IK. Polymer 1983;24(May):639–44.
[8] Kinloch AJ, Yuen ML, Jenkins SD. J Mater Sci 1994;29(14):3781–90.
[9] Young RJ, Beaumont PWR. J Mater Sci 1975;10:1343–50.
[10] Spanoudakis J, Young RJ. J Mater Sci 1984;19(2):473–86.
[11] Amdouni N, Sautereau H, Gerard JF. J Appl Polym Sci 1992;46(10):1723–35.
[12] Lee J, Yee AF. Polymer 2000;41:8363–73.
[13] Kawaguchi T, Pearson RA. Polymer 2003;44(15):4239–47.
[14] Kitey R, Tippur HV. Acta Mater 2005;53(4):1167–78.
[15] Kinloch AJ, Taylor AC, Lee JH, Sprenger S, Eger C, Egan D. J Adhes 2003;79(8–9):867–73.
[16] Kinloch AJ, Mohammed RD, Taylor AC, Eger C, Sprenger S, Egan D. J Mater Sci 2005;40(18):5083–6.
[17] Ragosta G, Abbate M, Musto P, Scarinzi G, Mascia L. Polymer 2005;46(23):10506–16.
[18] Zhang H, Zhang Z, Friedrich K, Eger C. Acta Mater 2006;54(7):1833–42.
[19] Sprenger S, Eger C, Kinloch AJ, Taylor AC, Lee JH, Egan D. Adhaesion Kleben Dichten 2003;2003(3):24–8.
[20] Hanse Chemie. Patent Application. WO 02/083776 A1, 2002.
[21] ISO-527-1. Plastics – determination of tensile properties – part 1: general principles. Geneva: ISO; 1993.
[22] ISO-527-2. Plastics – determination of tensile properties – part 2: test conditions for moulding and extrusion plastics. Geneva: ISO; 1996.
[23] ISO-13586. Plastics – determination of fracture toughness (G_{Ic} and K_{Ic}) – linear elastic fracture mechanics (LEFM) approach. Geneva: ISO; 2000.
[24] Kinloch AJ. Adhesion and adhesives: science and technology. London: Chapman & Hall; 1987.
[25] Johnsen BB, Kinloch AJ, Taylor AC. Polymer 2005;46(18):7352–69.
[26] Goodfellow product catalogue. Huntingdon: Goodfellow; 2005.
[27] Pascoe KJ. An introduction to the properties of engineering materials. 3rd ed. London: Van Nostrand Reinhold; 1978.
[28] Kerner EH. Proc Phys Soc B 1956;69:808–13.
[29] Nielsen LE. J Appl Polym Sci 1966;10:97–103.
[30] Halpin JC, Pagano NJ. J Compos Mater 1969;3:720–4.
[31] Ahmed S, Jones FR. J Mater Sci 1990;25(12):4933–42.
[32] Nielsen LE, Landel RF. Mechanical properties of polymers and composites. 2nd ed. New York: Marcel Dekker; 1994.
[33] Kinloch AJ, Taylor AC. J Mater Sci 2006;41(11):3271–97.
[34] Fornes TD, Paul DR. Polymer 2003;44(17):4993–5013.
[35] Luo J-J, Daniel IM. Compos Sci Technol 2003;63(11):1607–16.
[36] Halpin JC. J Compos Mater 1969;3:732–4.
[37] Halpin JC, Kardos JL. Polym Eng Sci 1976;186(5):344–52.
[38] Vollenberg PHT, Heikens D. Polymer 1989;30(9):1656–62.
[39] Lewis TB, Nielsen LE. J Appl Polym Sci 1970;14(6):1449–71.
[40] McGee S, McCullough RL. Polym Compos 1981;2(4):149–61.
[41] Nielsen LE. J Compos Mater 1968;2(1):120–3.
[42] Kinloch AJ, Taylor AC. J Mater Sci 2002;37(3):433–60.
[43] Andrews EH. Fracture in polymers. 1st ed. Edinburgh: Oliver & Boyd; 1968.
[44] Huang Y, Kinloch AJ. J Mater Sci 1992;27(10):2763–9.
[45] Kinloch AJ, Maxwell DL, Young RJ. J Mater Sci 1985;20(11):4169–84.
[46] Lange FF, Radford KC. J Mater Sci 1971;6(9):1197–203.
[47] Caddell RM. Deformation and fracture of solids. Englewood Cliffs, New Jersey: Prentice-Hall; 1980.
[48] Lange FF. Philos Mag 1970;22(179):983–92.
[49] Green DJ, Nicholson PS, Embury JD. J Mater Sci 1979;14(6):1413–20.
[50] Kinloch AJ, Young RJ. Fracture behaviour of polymers. London: Applied Science Publishers; 1983.
[51] Green DJ, Nicholson PS, Embury JD. J Mater Sci 1979;14(7):1657–61.
[52] Norman DA, Robertson RE. Polymer 2003;44(8):2351–62.
[53] Faber KT, Evans AG. Acta Metall 1983;31(4):565–76.
[54] Arakawa K, Takahashi K. Int J Frac 1995;48:103–14.
[55] Hull D. Fractography: observing, measuring, and interpreting fracture surface topography. Cambridge: Cambridge University Press; 1999.
[56] Hull D. J Mater Sci 1996;31(17):4483–92.
[57] Evans AG. Philos Mag 1972;26(6):1327–44.
[58] Odegard GM, Clancy TC, Gates TS. Polymer 2005;46(2):553–62.
[59] Rothon RN, Hancock M. General principles guiding selection and use of particulate materials. In: Rothon RN, editor. Particulate-filled polymer composites. Harlow: Longman Scientific & Technical; 1995. p. 1–45.
[60] Boluk MY, Schreiber HP. Polym Compos 1986;7(5):295–301.
[61] Iisaka K, Shibayama K. J Appl Polym Sci 1978;22(11):3135–43.
[62] Gerard JF, Amdouni N, Sautereau H, Pascault JP. Introduction of a rubbery interphase in glass/epoxy composite materials: influence of the interlayer thickness on the viscoelastic and mechanical properties of particulate and unidirectional composites. In: Ishida H, editor. Controlled interphases in composite materials. New York: Elsevier; 1990. p. 441–8.
[63] Iisaka K, Shibayama K. J Appl Polym Sci 1978;22:1845–52.
[64] Sultan JN, McGarry FJ. Polym Eng Sci 1973;13:29–34.
[65] Huang Y, Kinloch AJ. J Mater Sci 1992;27(10):2753–62.
[66] van Hartingsveldt EAA, van Aartsen JJ. Polymer 1989;30(11):1984–91.
[67] Vollenberg P, Heikens D, Ladan HCB. Polym Compos 1988;9(6):382–8.
[68] Pukanszky B, VanEs M, Maurer FHJ, Voros G. J Mater Sci 1994;29:2350–8.